








Radiation transport and scaling of optical depth in Nd:YAG laser-produced microdroplet-tin plasma

Cite as: Appl. Phys. Lett. **115**, 124101 (2019); <https://doi.org/10.1063/1.5117504>

Submitted: 02 July 2019 . Accepted: 05 September 2019 . Published Online: 19 September 2019

R. Schupp , F. Torretti , R. A. Meijer, M. Bayraktar , J. Sheil, J. Scheers , D. Kurilovich , A. Bayerle, A. A. Schafgans, M. Purvis, K. S. E. Eikema, S. Witte, W. Ubachs , R. Hoekstra, and O. O. Versolato 



View Online



Export Citation



CrossMark

ARTICLES YOU MAY BE INTERESTED IN

MOCVD epitaxy of β -(Al_xGa_{1-x})₂O₃ thin films on (010) Ga₂O₃ substrates and N-type doping
Applied Physics Letters **115**, 120602 (2019); <https://doi.org/10.1063/1.5123495>

Ambipolar transistor action of germanane electric double layer transistor
Applied Physics Letters **115**, 122101 (2019); <https://doi.org/10.1063/1.5094817>

Large metal halide perovskite crystals for field-effect transistor applications
Applied Physics Letters **115**, 120601 (2019); <https://doi.org/10.1063/1.5116411>

Lock-in Amplifiers up to 600 MHz

starting at
\$6,210



 Zurich
Instruments

Watch the Video 

Radiation transport and scaling of optical depth in Nd:YAG laser-produced microdroplet-tin plasma

Cite as: Appl. Phys. Lett. **115**, 124101 (2019); doi: [10.1063/1.5117504](https://doi.org/10.1063/1.5117504)

Submitted: 2 July 2019 · Accepted: 5 September 2019 ·

Published Online: 19 September 2019



View Online



Export Citation



CrossMark

R. Schupp,¹ F. Torretti,^{1,2} R. A. Meijer,^{1,2} M. Bayraktar,³ J. Sheil,¹ J. Scheers,^{1,2} D. Kurilovich,^{1,2} A. Bayerle,¹ A. A. Schafgans,⁴ M. Purvis,⁴ K. S. E. Eikema,^{1,2} S. Witte,^{1,2} W. Ubachs,^{1,2} R. Hoekstra,^{1,5} and O. O. Versolato^{1,a)}

AFFILIATIONS

¹Advanced Research Center for Nanolithography, Science Park 106, 1098 XG Amsterdam, The Netherlands

²Department of Physics and Astronomy, and LaserLaB, Vrije Universiteit, De Boelelaan 1081, 1081 HV Amsterdam, The Netherlands

³Industrial Focus Group XUV Optics, MESA+ Institute for Nanotechnology, University of Twente, Drienerlolaan 5, 7522 NB Enschede, The Netherlands

⁴ASML US LP, 17075 Thornmint Ct, San Diego, California 92127, USA

⁵Zernike Institute for Advanced Materials, University of Groningen, Nijenborgh 4, 9747 AG Groningen, The Netherlands

^{a)}Electronic mail: o.versolato@arcnl.nl

ABSTRACT

Experimental scaling relations of the optical depth are presented for the emission spectra of a tin-droplet-based, 1- μm -laser-produced plasma source of extreme-ultraviolet (EUV) light. The observed changes in the complex spectral emission of the plasma over a wide range of droplet diameters (16–65 μm) and laser pulse durations (5–25 ns) are accurately captured in a scaling relation featuring the optical depth of the plasma as a single, pertinent parameter. The scans were performed at a constant laser intensity of $1.4 \times 10^{11} \text{ W/cm}^2$, which maximizes the emission in a 2% bandwidth around 13.5 nm relative to the total spectral energy, the bandwidth relevant for industrial EUV lithography. Using a one-dimensional radiation transport model, the relative optical depth of the plasma is found to linearly increase with the droplet size with a slope that increases with the laser pulse duration. For small droplets and short laser pulses, the fraction of light emitted in the 2% bandwidth around 13.5 nm relative to the total spectral energy is shown to reach high values of more than 14%, which may enable conversion efficiencies of Nd:YAG laser light into—industrially—useful EUV radiation rivaling those of current state-of-the-art CO_2 -laser-driven sources.

© 2019 Author(s). All article content, except where otherwise noted, is licensed under a Creative Commons Attribution (CC BY) license (<http://creativecommons.org/licenses/by/4.0/>). <https://doi.org/10.1063/1.5117504>

The semiconductor industry is currently moving from deep-ultraviolet to extreme-ultraviolet (EUV) lithography for high-volume manufacturing of the next generation of microelectronics where the shorter wavelength of the EUV radiation enables further miniaturization. The light sources of choice for nanolithographic applications are laser-produced plasmas (LPPs).^{1–19} In these sources, tens-of-micrometer-sized tin droplets are irradiated by high-intensity (10^{10} W/cm^2) laser pulses in order to generate a high-density (10^{19} e/cm^3) plasma that efficiently emits EUV radiation.²⁰ Tin is used because several of its charge states have strong dipole transitions such as the $4d\text{--}4f$, $4p\text{--}4d$, and $4d\text{--}5p$ arrays in $\text{Sn}^{8\text{--}15+}$ which strongly emit around 13.5 nm,^{14,16} a wavelength that matches the peak reflectivity of the superfluous Mo/Si multilayer optics^{21,22} used in state-of-the-art EUV-lithography. The light of interest within a 2% bandwidth around 13.5 nm is referred to as “in-band” radiation.

Currently, CO_2 -gas lasers operating at a 10 μm wavelength are used to drive the EUV-emitting plasma, but with further developments regarding their output power, YAG solid-state lasers operating at 1 μm may become a viable alternative in the future. YAG laser systems provide a smaller footprint, a significantly higher efficiency in converting electrical power to laser light, and excellent temporal pulse shaping capabilities. The shorter 1 μm wavelength of YAG lasers gives rise to a 100 times higher critical plasma density ($n_{\text{crit}} \propto \lambda^{-2}$) compared to CO_2 -laser-driven plasmas, and higher laser intensities of typically 10^{11} W/cm^2 are needed to efficiently produce in-band radiation. The higher critical density results in a much higher, nearly complete absorption of the laser light by the tin target through the mechanism of inverse bremsstrahlung.^{23,24} A possible adverse effect of the higher critical plasma density is the creation of EUV radiation in plasma regions of higher density and repetition opacity. Significant self-absorption of

the emitted radiation can lead to a broadening of the spectral emission out of the 2% bandwidth of interest, thus reducing the spectral purity (SP) of the EUV plasma source.^{25–28} SP is defined as the ratio of in-band energy ($E_{ib,2\pi}$) over the total EUV energy ($E_{rad,2\pi}$) emitted into the half-sphere back toward the laser that is covered by multilayer optics in industrial sources. Conversion efficiency (CE) is defined as the ratio of the total produced EUV energy $E_{rad,2\pi}$ and the total incident laser energy. Considering conservation of energy, SP represents the absolute upper limit to the conversion efficiency: $CE \leq SP$, where CE approaches SP only if all light is emitted in the backward-facing 2π steradian and no laser energy is converted into other energy channels such as kinetic energy of charged particles.²⁹ A more stringent limit of $CE \leq SP/2$ is found in the case of spherically symmetric emission.²⁴ Given the importance of SP as an indicator for source performance, its scaling with relevant source parameters such as tin-droplet size, laser pulse duration, and laser beam spot size needs to be quantified and understood. The existing literature on Nd:YAG-laser-driven plasma from high-purity tin microdroplets,^{30–32} the industrial targets of choice, mainly focuses on the integrated amount of produced in-band emission rather than on the spectral properties of the plasma despite the importance of SP.

In this letter, a systematic study of the influence of the droplet size and laser pulse duration on the emission spectrum of a droplet-based, Nd:YAG-driven EUV source is presented. An analytical solution for radiation transport in an optically thick one-dimensional plasma is used to quantify opacity-driven broadening of key emission features.

In the experiment, spherical micrometer-sized liquid tin droplets were irradiated with high intensity laser pulses from a Nd:YAG laser system³³ operated at 1064 nm as described in Refs. 29 and 34. The laser pulse was temporally box shaped and of adjustable duration. It had a spatially flat-top shape of 96 μm diameter to homogeneously heat the plasma. The spectral emission from the plasma was observed with a transmission grating spectrometer³⁵ under 60° with respect to the incoming laser beam. The measured spectra were corrected for the grating's first and second order diffraction efficiency as well as for the quantum efficiency of the camera. After correction, the SP values were calculated with respect to the measured spectral range of 5.5–25.5 nm. The wavelength was calibrated in a separate experiment using atomic line emission from an aluminum plasma. Using a laser intensity of $1.4 \times 10^{11} \text{ W/cm}^2$ at which SP is optimal,²⁹ two sets of experiments were conducted.

First, spectra were measured for several laser pulse durations within the range of 5–25 ns while keeping the droplet size fixed at 46 μm . As seen in Fig. 1(a), the main emission feature at 13.5 nm broadens for a longer laser pulse duration, while all other spectral emission features remain remarkably similar even though the laser pulse duration was varied by a factor of five. This indicates that laser intensity is the pertinent parameter of the investigated LPP determining charge state distribution and temperature of the plasma.^{29,36}

Second, spectra were measured for various droplet sizes in the range of 16–65 μm at constant laser pulse durations of 5, 15, and 25 ns. Spectra for the 15 ns case are shown in Fig. 1(b). A striking similarity in the spectral structure is observed among plasmas formed on droplets of various sizes. With the increasing droplet size, the main spectral feature at 13.5 nm broadens and the short-wavelength radiation between 5.5 and 12 nm increases in intensity relative to the main emission feature.

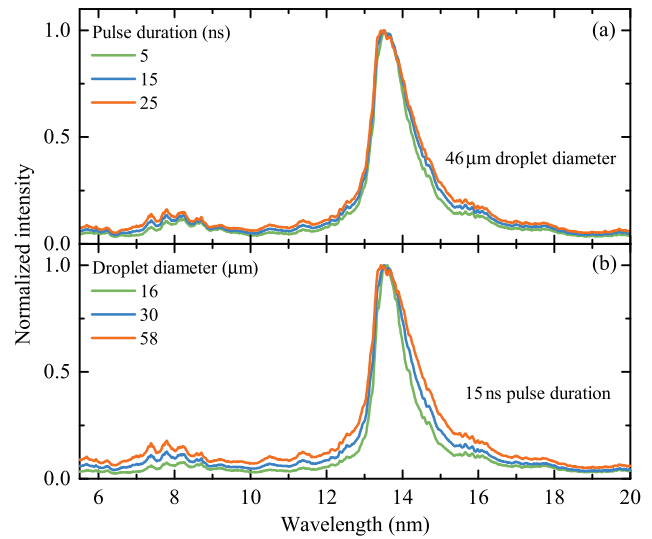


FIG. 1. Selection of emission spectra of Nd:YAG-laser-produced plasma from tin microdroplets irradiated at a constant laser intensity of $I = 1.4 \times 10^{11} \text{ W/cm}^2$ while varying either (a) the laser pulse duration or (b) the droplet diameter.

The observed broadening of spectral features for the increased pulse duration and droplet size, illustrated in Fig. 1, can be connected to an increase in the optical depth of the emitting plasma. The spectral radiance L_λ of a plasma with significant absorption and re-emission can be calculated using the equation of radiation transport. The subscript λ indicates the wavelength dependency of L_λ . The solution for a homogeneous one-dimensional plasma can be given in analytical form,³⁷

$$L_\lambda = S_\lambda(1 - e^{-\tau_\lambda}), \quad (1)$$

where $S_\lambda = j_\lambda/\alpha_\lambda$ is the source function defined by the ratio of emissivity j_λ and absorptivity α_λ . Opacity is given by $\kappa_\lambda = \alpha_\lambda/n_i$, where n_i is the ion density. In local thermodynamic equilibrium (LTE), where the atomic levels are thermally populated, the source function S_λ equals the Planck blackbody function B_λ . We assume that such LTE holds for the high-density, strongly collisional Nd:YAG-driven plasma. In the exponent, τ_λ is the wavelength-specific optical depth given by $\tau_\lambda = \int \alpha_\lambda dx$, where the absorptivity α_λ is integrated over the plasma length. Rearranging Eq. (1), the optical depth of the observed plasma can be obtained from its spectral radiance via

$$\tau_\lambda = -\ln\left(1 - \frac{L_\lambda}{B_\lambda}\right), \quad (2)$$

with the relative spectral radiance L_λ/B_λ . The optical depth of plasmas of the same temperature and density can only differ by a wavelength-independent factor a_i , here referred to as the relative optical depth, relating the plasmas' optical depths via $\tau_{\lambda,i} = a_i \tau_{\lambda,0}$. It follows from Eq. (2) that

$$\frac{L_{\lambda,i}}{B_\lambda} = 1 - \left(1 - \frac{L_{\lambda,0}}{B_\lambda}\right)^{a_i}. \quad (3)$$

It is instructive to use Eq. (3) to interpret the observed spectral changes, hypothesizing that the plasma length scale is the pertinent

parameter. At the wavelength λ_p of peak radiance near 13.5 nm, the optical depth typically has high values as follows from the work of Colgan *et al.*¹⁸ Their calculation results indicate a peak opacity value of $\sim 5 \times 10^5 \text{ cm}^2/\text{g}$ at a relevant ion density of 0.01 g/cm^3 . Thus, taking a reasonable $20 \mu\text{m}$ plasma length,²⁴ we deduce a typical value $\tau_{\lambda_p} \approx 10$. Next, as the plasma is heated under conditions of a spatially homogeneous laser illumination at constant intensity, we can ascribe to it a single, constant temperature. The entire plasma surface thus has a radiance L_{λ_i} (in units of $\text{W sr}^{-1} \text{ m}^{-2} \text{ Hz}^{-1}$) that is constant over the duration of the laser pulse. The observed spectra $O_{\lambda,i}$ can be related to L_{λ_i} by further realizing that an opaque plasma will have a spectral radiance equal to that of a blackbody $B_{\lambda,p}$ as here at a 13.5 nm wavelength ($\tau_{\lambda_p} \approx 10$). Thus, we equate $O_{\lambda,p}/B_{\lambda,p} := 1 = L_{\lambda,p}/B_{\lambda,p}$.

Using Eq. (3), any spectrum can be expressed in terms of any other spectrum via the relative optical depth a_i . The value of a_i can be obtained with respect to a chosen reference spectrum from a fit of Eq. (3) to the relative spectral radiance $L_{\lambda,i}/B_{\lambda}$. As a reference, for which $a_i = 1$, the relative spectral radiance $L_{\lambda,0}/B_{\lambda}$ of the spectrum with the narrowest main emission feature is used in the following, i.e., the one measured at a 5 ns pulse duration and a $16 \mu\text{m}$ droplet size. Typical literature values for the electron temperatures at which Nd:YAG LPPs most efficiently emit in-band radiation vary between 28 and 40 eV.^{18,24,38,39} A temperature in the center of this range of 34 eV is chosen for B_{λ} for all spectra. A common temperature is used because the laser intensity, which sets the effective plasma temperature, remains constant for all measurements. Variation of the blackbody temperature within the stated limits changes the fitted relative optical depth (see below) by less than 3%.

Figure 2 shows example data for $L_{\lambda,i}/B_{\lambda}$ vs $L_{\lambda,0}/B_{\lambda}$ for a wide range of droplet sizes and pulse durations. Excellent agreement of data and model fit is observed, featuring the relative optical depth a_i as a single free fit parameter.

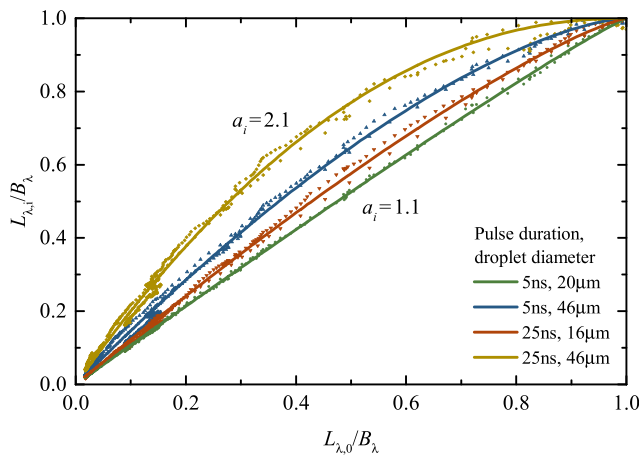


FIG. 2. Relative spectral radiance $L_{\lambda,i}/B_{\lambda}$ of experimental spectra taken at constant laser intensity but various laser pulse durations and droplet sizes (cf. Fig. 1). The relative spectral radiances are plotted as dotted curves with respect to the one of a reference spectrum $L_{\lambda,0}/B_{\lambda}$ obtained at a 5 ns laser pulse duration and a $16 \mu\text{m}$ droplet diameter where the main emission feature at 13.5 nm is the narrowest. For the blackbody function B_{λ} , a temperature of 34 eV was used. The solid lines depict fits of Eq. (3) to the data featuring the relative optical depth a_i as the single free fit parameter.

The values of the relative optical depth a_i as obtained from the procedure shown in Fig. 2 enable reproduction of spectra measured for other droplet sizes and laser pulse durations by radiation transport of the reference spectrum. Inserting the relative optical depth obtained from the fits into Eq. (3) and multiplying by B_{λ} lead to an excellent reproduction of experimental spectra as seen in Figs. 3(a) and 3(b). This is especially true for the main emission feature around 13.5 nm. When comparing the transported spectrum in the short-wavelength region between 5 and 12 nm, minor differences are visible. The differences are very small for the increasing pulse duration in Fig. 3(a) and become slightly more pronounced for the increasing droplet size in Fig. 3(b). This may be explained by changes in the plasma other than a simple linear optical depth such as emission from a multitemperature plasma or a slight dependence of plasma charge state distribution with the droplet size and pulse duration. Comparison of the relative intensities of the short-wavelength features suggests that the average charge state slightly increases with the droplet size.^{29,40} To account for a possibly higher average charge state of the plasma at a longer pulse duration and larger droplet size, the scaled reference spectrum may instead be compared to spectra taken at lower laser intensity. Indeed, comparison with spectra taken at a laser intensity of $1.1 \times 10^{11} \text{ W/cm}^2$ shows excellent agreement over the entire spectral range measured. We thus observe that the short-wavelength band between 5 and 12 nm is a much more sensitive probe to the emission properties of Sn LPPs than the main emission feature at 13.5 nm.

In Fig. 4(a), the fitted values for spectra of all pulse durations and droplet sizes are summarized. The relative optical depth a_i appears to scale linearly with the droplet radius and to strongly depend on the pulse duration. Linear fits are in good agreement with the data and converge to a common intercept of ~ 0.7 at zero droplet diameter. The

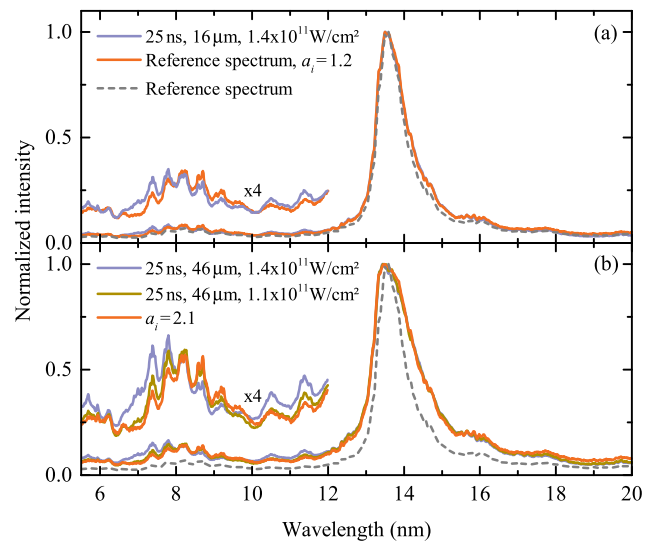


FIG. 3. Comparison of the reference spectrum and radiation transported reference spectrum with the measured spectra. The reference spectrum was transported using Eq. (3) together with the relative optical depth as determined in Fig. 2. (a) Increasing laser pulse duration. (b) Increasing laser pulse duration and droplet size. An additional spectrum is shown measured at a lower laser intensity of $1.1 \times 10^{11} \text{ W/cm}^2$, providing a better match with the radiation transported spectrum in the 5–12 nm range.

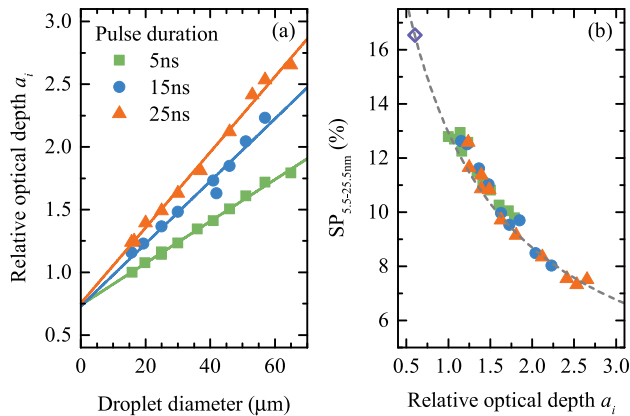


FIG. 4. (a) Dependency of the relative optical depth a_i on the droplet diameter for various laser pulse durations as obtained, e.g., in Fig. 2. The solid lines show a linear extrapolation of the data toward zero droplet size. (b) Experimental values for spectral purity ($SP_{5.5-25.5nm}$) vs relative optical depth. The dashed line represents $SP_{5.5-25.5nm}$ as calculated from the radiation transported reference spectrum. The open diamond symbol indicates the $SP_{5.5-25.5nm}$ value of the radiation transported reference spectrum for a relative optical depth parameter $a_i = 0.6$, a value obtained from comparison of the radiation transported reference spectrum with the emission of the CO_2 -laser-driven plasma as shown in Fig. 5 (see the text).

slope coefficients monotonically increase with the pulse duration from 0.017 to 0.025 and 0.030 μm^{-1} for 5, 15, and 25 ns, respectively.

Having identified the optical depth as the pertinent scaling parameter for Nd:YAG-laser-produced tin plasmas, the spectral purity of the emission spectrum is related to it in Fig. 4(b). Using this scaling, all experimental $SP_{5.5-25.5nm}$ values, calculated over a range of 5.5–25.5 nm as denoted in the subscript, collapse onto the gray dashed curve obtained by calculating the $SP_{5.5-25.5nm}$ of the radiation transported reference spectrum.

It is instructive to compare the $SP_{5.5-25.5nm}$ scaling captured by the gray dashed curve with the SP value of spectra from a state-of-the-art, CO_2 -laser-driven EUV source. Such CO_2 -laser-driven plasmas may be expected to have small optical depths $\tau < 1$ and thus less broadening, considering the 100-fold decrease in critical density compared to the Nd:YAG case. These CO_2 -laser-driven sources are, in general, characterized by relatively high SP and CE values. The spectrum was obtained (see Fig. 5) by predefining a droplet by a low intensity CO_2 laser “prepulse,” leading to a disk-shaped target of approximately 200 μm in diameter. The flat target was subsequently irradiated by a high-intensity, 100 ns, 320 mJ “main pulse” with a beam size that matched the target to produce EUV radiation. In this case, the spectrum was taken over a wavelength band spanning 6.8–16.7 nm. The fraction of light emitted in the 2% bandwidth around 13.5 nm relative to the total spectral energy in this measured bandwidth is $SP_{6.8nm-16.7nm} = 23\%$. For a relative optical depth $a_i = 0.6$, the Nd:YAG reference spectrum is found to closely match this $SP_{6.8nm-16.7nm}$ performance (also see Fig. 5). Over the extended wavelength band of 5.5–25.5 nm that defines SP in this work, this scaled Nd:YAG LPP spectrum has $SP_{5.5-25.5nm} = 16.5\%$ [open diamond symbol in Fig. 4(b)]. This is a remarkable finding as the plasma conditions for the two cases are vastly different and the conditions of LTE and $\tau \gg 1$ required for the procedure outlined in this work are not met for the CO_2 case.

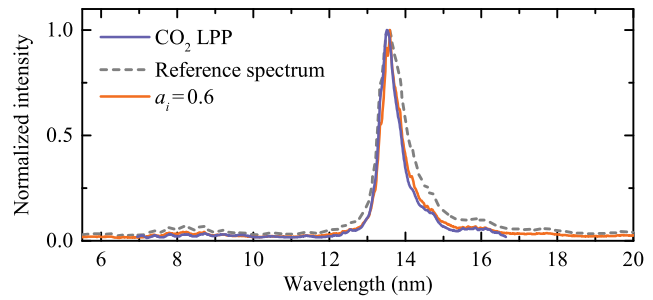


FIG. 5. Comparison of the transported reference spectrum using Eq. (3) with $a_i = 0.6$ and the spectral emission from a CO_2 -laser-driven plasma.

Calculating the maximally obtainable conversion efficiency via $CE = SP/2$,^{24,29} a significantly higher CE value is expected for CO_2 -driven LPPs, given its higher SP. However, accounting for the fraction of laser light ϵ absorbed by the tin target—near unity (>0.9)⁴¹ for the case of 1 μm radiation, while about 0.7 for 10 μm light⁴²—both drive laser cases may indeed have about the same conversion efficiency limit of $CE = \epsilon SP_{5.5-25.5nm}/2 \approx 6\%$ making 1 μm solid state lasers a viable alternative as source drive lasers. Naturally, the maximum obtainable CE depends not only on the emission spectrum as there are further significant contributions to the total energy balance, aside from a finite emission anisotropy. Examples include plasma kinetics, ionization energy, and contributions from plasma emission outside the 5.5–25.5 nm range. A careful comparison of this total energy balance is required between the CO_2 and Nd:YAG drive laser cases. Further, a central requirement is the creation of manageable amounts of debris from the plasma. This entails, among others, fragments or high-energy particles that could reduce optics lifetime. Laser energy not contributing to radiation may instead lead to the production of fast ionic debris, and possible gains in spectral purity and radiative output power should be carefully weighed out against, e.g., increases in the tin load on the optical components. A full quantification of the loads of various debris is left for future work.

In conclusion, the optical depth is established to be the pertinent scaling parameter in high-density laser-produced plasmas from tin-microdroplets. The observed changes in the experimental emission spectra from plasmas of various droplet sizes as well as various laser pulse durations are remarkably well described using a one-dimensional radiation transport equation featuring the relative optical depth of the plasma as the sole parameter. The excellent description of the experimental data by the model suggests that a dominant fraction of the EUV emission may be produced in a single-density, single-temperature region of the plasma because the underlying opacity does not appear to change. The here established scaling with the optical depth indicates that Nd:YAG LPPs may suffer from strong absorption and re-emission significantly redistributing the spectral energy into wavelength-bands other than 13.5 nm in the case of large plasma size. Therefore, the optical depth of these light sources needs to be minimized to reach the highest SP values which can be done by reduction of the laser pulse duration and droplet size. In such optimized cases, and accounting for the difference in laser absorptivity, CE values of Nd:YAG-laser-driven plasma may well rival those of state-of-the-art CO_2 -laser-driven plasma sources.

This work was carried out at the Advanced Research Center for Nanolithography (ARCNL), a public-private partnership of the University of Amsterdam (UvA), the Vrije Universiteit Amsterdam (VU), the Netherlands Organisation for Scientific Research (NWO), and the semiconductor equipment manufacturer ASML. The part of this work concerning the CO₂-laser-produced plasma was carried out at the ASML San Diego part of ASML U.S. LP. The used transmission grating spectrometer has been developed in the Industrial Focus Group XUV Optics at the University of Twente and supported by the FOM Valorisation Prize 2011 awarded to F. Bijkerk and NanoNextNL Valorization Grant awarded to M. Bayraktar in 2015. This project received funding from the European Research Council (ERC) Starting Grant No. 802648 and is part of the VIDII research programme with Project No. 15697, which is financed by NWO.

REFERENCES

- ¹O. O. Versolato, *Plasma Sources Sci. Technol.* **28**, 083001 (2019).
- ²M. Purvis, I. V. Fomenkov, A. A. Schafgans, M. Vargas, S. Rich, Y. Tao, S. I. Rokitski, M. Mulder, E. Buurman, M. Kats *et al.*, *Proc. SPIE* **10583**, 1058327 (2018).
- ³S. K. Moore, *IEEE Spectrum* **55**, 46 (2018).
- ⁴A. A. Schafgans, D. J. Brown, I. V. Fomenkov, R. Sandstrom, A. Ershov, G. Vaschenko, R. Rafac, M. Purvis, S. Rokitski, Y. Tao *et al.*, *Proc. SPIE* **9422**, 94220B (2015).
- ⁵V. I. Azarov and Y. N. Joshi, *J. Phys. B: At. Mol. Opt. Phys.* **26**, 3495 (1993).
- ⁶W. Svendsen and G. O'Sullivan, *Phys. Rev. A* **50**, 3710 (1994).
- ⁷S. S. Churilov and A. N. Ryabtsev, *Phys. Scr.* **73**, 614 (2006).
- ⁸S. S. Churilov and A. N. Ryabtsev, *Opt. Spectrosc.* **100**, 660 (2006).
- ⁹S. S. Churilov and A. N. Ryabtsev, *Opt. Spectrosc.* **101**, 169 (2006).
- ¹⁰A. N. Ryabtsev, É. Y. Kononov, and S. S. Churilov, *Opt. Spectrosc.* **105**, 844 (2008).
- ¹¹I. Y. Tolstikhina, S. S. Churilov, A. N. Ryabtsev, and K. N. Koshelev, in *EUV Sources for Lithography*, edited by V. Bakshi (SPIE Press, 2006), Chap. 4, pp. 113–148.
- ¹²J. Benschop, V. Banine, S. Lok, and E. Loopstra, *J. Vac. Sci. Technol., B* **26**, 2204 (2008).
- ¹³R. D'Arcy, H. Ohashi, S. Suda, H. Tanuma, S. Fujioka, H. Nishimura, K. Nishihara, C. Suzuki, T. Kato, F. Koike, J. White, and G. O'Sullivan, *Phys. Rev. A* **79**, 042509 (2009).
- ¹⁴H. Ohashi, S. Suda, H. Tanuma, S. Fujioka, H. Nishimura, A. Sasaki, and K. Nishihara, *J. Phys. B: At. Mol. Opt. Phys.* **43**, 065204 (2010).
- ¹⁵V. Y. Banine, K. N. Koshelev, and G. H. P. M. Swinkels, *J. Phys. D: Appl. Phys.* **44**, 253001 (2011).
- ¹⁶G. O'Sullivan, B. Li, R. D'Arcy, P. Dunne, P. Hayden, D. Kilbane, T. McCormack, H. Ohashi, F. O'Reilly, P. Sheridan, E. Sokell, C. Suzuki, and T. Higashiguchi, *J. Phys. B: At. Mol. Opt. Phys.* **48**, 144025 (2015).
- ¹⁷A. Windberger, F. Torretti, A. Borschevsky, A. Ryabtsev, S. Dobrodey, H. Bekker, E. Eliav, U. Kaldor, W. Ubachs, R. Hoekstra, J. R. Crespo López-Urrutia, and O. O. Versolato, *Phys. Rev. A* **94**, 012506 (2016).
- ¹⁸J. Colgan, D. Kilcrease, J. Abdallah, M. Sherrill, C. Fontes, P. Hakel, and G. Armstrong, *High Energy Density Phys.* **23**, 133 (2017).
- ¹⁹F. Torretti, A. Windberger, A. Ryabtsev, S. Dobrodey, H. Bekker, W. Ubachs, R. Hoekstra, E. V. Kahl, J. C. Berengut, J. R. C. López-Urrutia, and O. O. Versolato, *Phys. Rev. A* **95**, 042503 (2017).
- ²⁰M. A. Purvis, A. Schafgans, D. J. Brown, I. Fomenkov, R. Rafac, J. Brown, Y. Tao, S. Rokitski, M. Abraham, M. Vargas *et al.*, *Proc. SPIE* **9776**, 97760K (2016).
- ²¹S. Bajt, J. B. Alameda, T. W. Barbee, Jr., W. M. Clift, J. A. Foltz, B. Kaufmann, and E. A. Spiller, *Opt. Eng.* **41**, 1797 (2002).
- ²²Q. Huang, V. Medvedev, R. van de Kruijs, A. Yakshin, E. Louis, and F. Bijkerk, *Appl. Phys. Rev.* **4**, 011104 (2017).
- ²³P. Mora, *Phys. Fluids* **25**, 1051 (1982).
- ²⁴M. Basko, *Phys. Plasmas* **23**, 083114 (2016).
- ²⁵S. Fujioka, H. Nishimura, K. Nishihara, A. Sasaki, A. Sunahara, T. Okuno, N. Ueda, T. Ando, Y. Tao, Y. Shimada, K. Hashimoto, M. Yamaura, K. Shigemori, M. Nakai, K. Nagai, T. Norimatsu, T. Nishikawa, N. Miyanaga, Y. Izawa, and K. Mima, *Phys. Rev. Lett.* **95**, 235004 (2005).
- ²⁶H. Tanaka, A. Matsumoto, K. Akinaga, A. Takahashi, and T. Okada, *Appl. Phys. Lett.* **87**, 041503 (2005).
- ²⁷P. Hayden, A. Cummings, N. Murphy, G. O'Sullivan, P. Sheridan, J. White, and P. Dunne, *J. Appl. Phys.* **99**, 093302 (2006).
- ²⁸J. White, P. Dunne, P. Hayden, F. O'Reilly, and G. O'Sullivan, *Appl. Phys. Lett.* **90**, 181502 (2007).
- ²⁹R. Schupp, F. Torretti, R. A. Meijer, M. Bayraktar, J. Scheers, D. Kurilovich, A. Bayerle, K. S. E. Eikema, S. Witte, W. Ubachs, R. Hoekstra, and O. O. Versolato, *Phys. Rev. Appl.* **12**, 014010 (2019).
- ³⁰A. Z. Giovannini and R. S. Abhari, *J. Appl. Phys.* **114**, 033303 (2013).
- ³¹A. Z. Giovannini and R. S. Abhari, *Appl. Phys. Lett.* **104**, 194104 (2014).
- ³²H. Chen, X. Wang, L. Duan, H. Lan, Z. Chen, D. Zuo, and P. Lu, *J. Appl. Phys.* **117**, 193302 (2015).
- ³³R. A. Meijer, A. S. Stodolna, K. S. E. Eikema, and S. Witte, *Opt. Lett.* **42**, 2758 (2017).
- ³⁴D. Kurilovich, A. L. Klein, F. Torretti, A. Lassise, R. Hoekstra, W. Ubachs, H. Gelderblom, and O. O. Versolato, *Phys. Rev. Appl.* **6**, 014018 (2016).
- ³⁵M. Bayraktar, H. M. Bastiaens, C. Bruineman, B. Vratzov, and F. Bijkerk, *NEVAC blad* **54**, 14 (2016).
- ³⁶D. Colombant and G. Tonon, *J. Appl. Phys.* **44**, 3524 (1973).
- ³⁷V. Bakshi *et al.*, *EUV Sources for Lithography* (SPIE Press, Bellingham, Washington, 2006), Vol. 149.
- ³⁸M. Murakami, S. Fujioka, H. Nishimura, T. Ando, N. Ueda, Y. Shimada, and M. Yamaura, *Phys. Plasmas* **13**, 033107 (2006).
- ³⁹A. Hassanein, V. A. Sizyuk, T. S. Sizyuk, and S. Harilal, *J. Micro/Nanolithogr., MEMS, MOEMS* **8**, 041503 (2009).
- ⁴⁰F. Torretti, R. Schupp, D. Kurilovich, A. Bayerle, J. Scheers, W. Ubachs, R. Hoekstra, and O. Versolato, *J. Phys. B: At. Mol. Opt. Phys.* **51**, 045005 (2018).
- ⁴¹D. Kurilovich, M. M. Basko, D. A. Kim, F. Torretti, R. Schupp, J. C. Visschers, J. Scheers, R. Hoekstra, W. Ubachs, and O. O. Versolato, *Phys. Plasmas* **25**, 012709 (2018).
- ⁴²A. Hassanein, T. Sizyuk, V. Sizyuk, and S. Harilal, *Proc. SPIE* **7969**, 79690D (2011).